

## Computing Strain Rate Sensitivity of Aluminium Alloy 1050

Mohammad Reza Allazadeh

Advanced Forming Research Centre, Inchinnan, Renfrew, The United Kingdom

**Abstract.** The strain rate sensitivity of commercial aluminium alloy 1050 (or AA1050) was calculated using uniaxial tensile test results. The experimental data were collected from hot uniaxial tensile test carried out according to E-2448 standard at different strain rates and testing temperatures. The results were analysed to approximate the optimum value of strain rate sensitivity (m-value) for commercial AA1050 tempering H14 with no additional heat treatment or microstructure altering. The strain rate sensitivity was determined by implementing the uniaxial tensile test data in creep law and by plotting the strain rate-flow stress curve. The formulation of the problem was demonstrated for Bailey-Norton law time hardening and strain hardening governing equations. The results presented low strain rate sensitivity of AA1050-H14 at 100 °C, 200 °C, 300 °C, and 500 °C for the selected pure plastic strains before necking zone. The maximum m-value for uniaxial tensile tests was found to be about the probe strain of 4% at 300 °C forming temperature under loading with the strain rate of 0.0005 s<sup>-1</sup>.

**Key words:** strain rate sensitivity, m-value, aluminium alloy 1050, sheet forming process, creep flow stress, computational model, uniaxial tensile test.

### Introduction

Aluminium alloy 1050 has several industrial manufacturing specification, such as AA1050, Al1050, A91050, and S1B. It is one of the most popular aluminium grades in industry due to its relatively low price, surface chemical resistance, good formability, moderate strength, and high reflective finish (Metals4U LTD, 2019). Like other 1xxx series aluminium alloys, AA1050 is among the purest commercial aluminium grades with 99% pure aluminium in its chemical composition. Al1050 has excellent anticorrosive and ductility attributes but its high aluminium content deteriorates considerably its machinability and results in material clogging on the tools and cutters (Aalco Metals Ltd, 2011). For that reason, its major products are shaped by sheet metal forming processes. Commercial AA1050 sheets are usually supplied without any heat treatment and ultrafine grain microstructural evolution, and therefore, it is suitable for low strain forming process. AA1050 has applications in food industry, automotive industry, architecture, pharmaceutical industry, chemical industry, packaging, and general sheet metal work (Smiths Metal Centres, 2018). Commercial Al1050 is very often available in H14 temper, which is designed for cold working and forming. The temper H14 indicates that the aluminium sheets is rolled to improve their hardness by 50% via work hardening instead of annealing process (Aalco Metals Ltd, 2011). Nevertheless, it is possible to improve metal stretching properties by grain refinements techniques, e.g. high-pressure torsion (HPT), accumulative roll-bonding (ARB) process, and equal channel angular extrusion (ECAE) (Kima et al., 2017: 26-32). Grain refinements techniques increase highly the final price of Al1050 products. This drives the relevant industrial sectors to inquire about the optimum forming parameters for industrial scale productions.

In general, strain rate and temperature are two main parameters controlling the production rate and formability of the metal product, respectively. Combination of these parameters contribute to the ability of the sheet to stretch during sheet forming processes.

It is fair to say the mechanical properties of a specific aluminium alloy determine its application but it is also necessary to consider material workability in product manufacturing (Zheng et al., 2018: 55-80). The workability of metal alloys is related to manufacturing parameters through several formability parameters. One of the main factors influencing material workability is strain rate sensitivity index, also known as *m-value*, which helps to evaluate the extent of inelastic deformation of a material. The strain rate sensitivity is particularly important in sheet-forming operations to describe the strain distribution effect and necking resistance caused by the dependencies of flow strength to strain-hardening behaviour. This relationship is captured in the definition of *m-value* by the ratio of the flow stress variation to the change in the strain rate for certain forming temperature and about a predefined plastic strain.

Totten and Mackenzie argued that high stretchability of aluminium alloy may attain under slow flow stress loading for aluminium sheets with very fine and stable grains whose *m-values* is above 0.4 (Totten and Mackenzie, 2003: 1105-1114). These conditions are not expected in commercial AA1050 under conventional forming conditions, however, the information about *m-value* of AA1050 can extend its application in the industry, particularly in production of light weight components. Studying strain rate sensitivity of aluminium alloys was subject of many literatures for wide ranges of forming temperatures and strain rates (Picua, 2005: 334-343; Chen et al., 2009: 3825-3835; Majidi, 2017: 020022; Khan and Liu, 2012: 1-14; Lademo et al., 2010: 041007). However, these studies were mainly focus on AA2xxx, AA3xxx, AA5xxx, AA6xxx, and AA7xxx due to their wide applications in aerospace and automobiles industries. Few researchers have discussed the strain rate sensitivities of AA1xxx series (Lademo et al., 2010: 041007; Huang and Khan, 1992: 501-517), however, their investigations were not included AA1050 *m-value*. Mohebbi et al. investigated the stress relaxation (SR) effect on the *m-value* of ultrafine grain (UFG) AA1050 at the ambient temperature without considering its alteration at the elevated temperature (Mohebbi and Akbarzadeh, 2017: 167-176). Different material properties of commercial AA1050 can be found in several journal articles (Bolt et al., 2001: 118-121; Demirci et al., 2008: 526-532; Afshin and Kadkhodayan, 2015: 25-35; Morais, 2014) and manufacturing datasheets (Metals4U LTD, 2019; Aalco Metals Ltd, 2019; Grupo Andaluca, 2013), but it is hard to find publications on its *m-value* computation.

Several uniaxial tensile test were performed for AA1050-H14 at different strain rates and forming temperatures using SPF specimens to compute its strain rate sensitivity at different forming temperature. The uniaxial tensile test results were carried out according to E-2448 standard at 100 °C, 200 °C, 300 °C, and 500 °C about different selected plastic strains. The aforementioned uniaxial tensile test results showed that the plastic material flow of Al1050 has some degrees of sensitivity to the strain rate. Secondary creep model was deployed as governing equation to predict the stress-strain relationship for AA1050 sheet forming process. The AA1050 sheets` ability to stretch was scrutinised to obtain the optimum temperature for its forming. This paper facilitates to determine the forming criteria of AA1050 in the industry and provides the strain rate sensitivity of aluminium alloy 1050 to the researchers on this topic.

### Uniaxial tensile test experiments

The uniaxial tensile test coupons were designed for commercial aluminium alloy sheet AA1050-H14 with specification of BS EN 573-3:2009 and thickness of  $2\pm 0.1$  mm.

The experiments were executed following E-2448 regulations and steps in Zwick/Roell Z250 strength testing device. The selected sheet was inspected prior to be cut to make the test coupons to ensure it is free of even minor damage or scratch on its surfaces.

Table 1. Uniaxial tensile tests` specifications for the experiments

Uniaxial tensile test coupon ID	Testing Temperature [°C]	Strain Rate [s <sup>-1</sup> ]	Rolling Direction [degree]
J	100	0.005	90
I	200	0.001	90
H	200	0.0005	90
E	200	0.0001	90
K	300	0.001	90
L	300	0.0005	0
O	300	0.0005	45
G	300	0.0005	90
M	300	0.0001	0
N	300	0.0001	45
F	300	0.0001	90
T	400	0.0001	90
S	500	0.001	90
D	500	0.005	90
Q	500	0.0005	90
R	500	0.0001	90

Table 1 provides the detail of the uniaxial tensile test parameters for each specimen labelled with an identification letter. The selected temperatures for the uniaxial tensile tests were 100 °C, 200 °C, 300 °C, 400 °C, and 500 °C. The strain rates of the tests were set to be 0.0001, 0.005, 0.001, and 0.005 s<sup>-1</sup>. Fig. 1 presents all the resultant graphs from the uniaxial tensile tests carried to obtain the true stress versus true strain curves to compute m-value of AA1050-H14. The author has discussed the results in more detail in (Allazadeh, 2018: 9009).

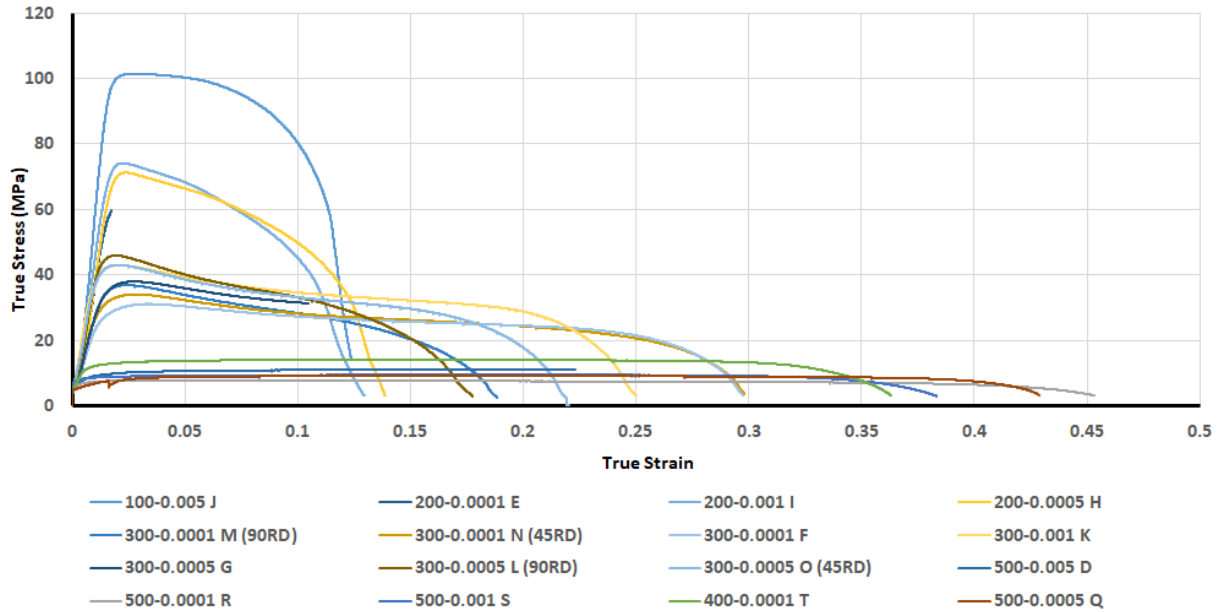


Fig 1. The uniaxial tensile test results of the samples cut from AA1050-H14 sheets to compute its m-value

**Formulation of strain rate sensitivity**

It can be concluded from analysing the effect of the strain rate on the true stress-true strain curves in Fig. 1 that Al1050 material flow follows creep behaviour during the hot uniaxial tensile tests. Therefore, one may predict the stress flow within the material during the forming process using one of the creep models.

Creep models can be categorised into three models of primary, secondary, and tertiary creeps, which are fit for non-proportional response, proportional response, and hardening, respectively. Usually, secondary creep is the acceptable material model for the major unspecified creep behaviours since it is predominate creep and it has compatibility with wider range for forming applications (San-Vicente, 2004). Secondary creep model is formulated as,

$$\dot{\epsilon}^{cr} = A\sigma^m \tag{1}$$

Parameters  $\sigma$  and  $\epsilon$  in equation (1) are presenting the stress flow and material creep during deformation process, respectively.  $A$  and  $m$  parameters in equation (1) are the constants determining the strain hardening behaviour. The strain rate  $\dot{\epsilon}^{cr}$  is the specific strain rate for the creep under flow stress  $\sigma$ , which provides the maximum ductility. The ductility of the material is reduced for any strain rate higher or lower than creep strain rate  $\dot{\epsilon}^{cr}$ . It can be realised from equation (1) that strain rate is the primary factor for the rate of change in flow stress. This phenomenon is known as strain rate sensitivity and measured as m-value for the given strain and temperature with the following formula,

$$m = \left. \frac{\delta \ln \sigma}{\delta \ln \dot{\epsilon}^{cr}} \right|_{T, \epsilon} \tag{2}$$

It is worth to mention that microstructure of material affects m-value of material such that smaller grain size generally leads to lower flow stresses, higher values of strain-rate

sensitivity ( $m$ ), and greater ductility (San-Vicente, 2004; Hamilton et al., 1985: 172-190; Bae and Ghosh, 2000: 1207-1224; Mukherjee, 1993: 408–456). Bailey and Norton have introduced a time-dependent model for plastic deformation, which very often is used for the primary and secondary creep regimes as in equation (3) (Betten, 2008: 52),

$$\dot{\epsilon}^{cr} = A\sigma^n t^k \tag{3}$$

It is possible to show that stress exponent,  $n$ , is equal to  $1/m$  (See Appendix A). Creep strain rate  $\dot{\epsilon}^{cr}$  is the corresponding strain rate to the true stress  $\sigma$  and creep strain,  $\epsilon^{cr}$ , with largest plastic elongation before necking instigation. Moreover, since power law equation (3) is separable to different independent functions, it is plausible to use regression analysis to calculate the dependent and independent variable  $\epsilon$ ,  $\sigma$ ,  $A$ ,  $n$ ,  $k$  (May et al., 2013). Appendix B shows that equation

(3) can be rearranged to derive strain rate form of Bailey-Norton law time hardening expression as next,

$$\dot{\epsilon}^{cr} = A'\sigma'^n t'^k \tag{4}$$

Appendix B also gives the equations to calculate temperature dependent constants  $A'$ ,  $n'$ , and  $k'$ . Parameter  $t'$  is the total time of the creep deformation.  $\sigma'$  is the uniaxial deviatoric stress for the creep strain rate  $\dot{\epsilon}_{cr}$ . Unit of coefficient  $A'$  is determined by the units of creep's time and stress in the formula. Subsequently, the strain hardening form of creep law can be derived from time hardening constitutive model in equation

(4) (See the detail in Appendix C). The strain hardening governing equation for creep law is,

$$\dot{\epsilon}^{cr} = \{A'\sigma'^n [(m' + 1)\epsilon]^{k'}\}^{\frac{1}{k'+1}} \tag{5}$$

Appendix C gives the details of computing  $A'$ ,  $n'$ , and  $k'$  in equation (5).

### Results and Discussion

The values of the strain rate sensitivity are calculated for AA1050- H14 at 100 °C, 200 °C, 300 °C, and 500 °C. The material designation H is usually followed by two or more numbers and applied for products that have been strengthened by strain hardening, with or without subsequent heat treatment. The strain rate sensitivity index ( $m$ -value) was calculated at several specific strains within the pure plastic deformation zone before necking initiation.

Since the value of  $m$  index is determined by both strain and strain rate, therefore, its corresponding temperature, strain, and strain rate must be specified in a quoted value as well (Betten, 2008: 52). Equation (2) is employed to use the uniaxial tensile test experiments in Fig. 1 to evaluate the  $m$ -value at different temperatures.

Table 2. Strain rate calculation parameters at 200 °C about strain value of 0.025, 0.04, 0.05, and 0.6

T [°C]	$\epsilon$	$\dot{\epsilon}_1$ [s <sup>-1</sup> ]	$\dot{\epsilon}_2$ [s <sup>-1</sup> ]	$\sigma_1$ [MPa]	$\sigma_2$ [MPa]	$m$	$m_{ave}(\epsilon, T)$
--------	------------	---------------------------------------	---------------------------------------	------------------	------------------	-----	------------------------

200	0.025	0.0001	0.001	62.47	73.8	0.073	0.069
200	0.025	0.0001	0.0005	62.47	71.1	0.081	
200	0.04	0.0001	0.001	59.50	70.71	0.075	0.073
200	0.04	0.0001	0.0005	59.50	67.73	0.081	
200	0.04	0.0005	0.001	67.73	70.714	0.062	
200	0.05	0.0001	0.001	57.74	68.30	0.073	0.080
200	0.05	0.0001	0.0005	57.74	66.36	0.086	
200	0.06	0.0001	0.001	55.96	64.95	0.065	0.075
200	0.06	0.0001	0.0005	55.96	64.17	0.085	

Following ASTM E 2448 standard, the strain rate sensitivity was calculated at specific creep strains within the plastic deformation zone before necking initiation at 200 °C, 300 °C, and 500 °C. Strain rate sensitivity varies during deformation since it is governed by the overall deformation and stability during forming process. This results in changing of the thickness due to the strain variation during formation (Nazzal et al., 2007: 189-192). It is due to that fact that the strain may reach well over the selected strain level, and subsequently, the strain variation may cause the changes in the cross-section of material and thickness variation (Mishra et al., 2004). Table 2 lists the computed values of the strain rate sensitivity at 200°C, along with their corresponding parameters, for the stress flow about strain value of 0.025, 0.04, 0.05, and 0.06.

Table 3 contains the m-values and their computational parameters at 300 °C about the strains value of 0.04, 0.05, and 0.1. Table 4 shows the m-values at 500 °C for the stress flow about the strain value of 0.0001, 0.0005, 0.001, and 0.005. In addition, Table 2, Table 3, and Table 4 offer the average m-value for different strain rates about a particular strain and forming temperature.

Table 3. Strain rate calculation parameters at 300 °C about strain value of 0.04, 0.05, 0.6, and 0.1

T [°C]	$\epsilon$	$\dot{\epsilon}_1$ [s <sup>-1</sup> ]	$\dot{\epsilon}_2$ [s <sup>-1</sup> ]	$\sigma_1$ [MPa]	$\sigma_2$ [MPa]	m	$m_{ave}(\epsilon, T)$
300	0.04	0.0001	0.001	30.90	40.66	0.119	0.123
300	0.04	0.0001	0.0005	30.90	36.94	0.111	
300	0.04	0.0005	0.001	36.94	40.66	0.138	
300	0.05	0.0001	0.001	30.39	39.36	0.112	0.116
300	0.05	0.0001	0.0005	30.39	35.90	0.103	
300	0.05	0.0005	0.001	35.90	39.36	0.133	
300	0.1	0.0001	0.001	27.32	34.64	0.103	0.109
300	0.1	0.0001	0.0005	27.32	31.58	0.090	
300	0.1	0.0005	0.001	31.58	34.64	0.134	

Table 4. Strain rate calculation parameters at 500 °C about strain value of 0.0001, 0.0005, 0.001, and 0.005

T [°C]	$\epsilon$	$\dot{\epsilon}_1$ [s <sup>-1</sup> ]	$\dot{\epsilon}_2$ [s <sup>-1</sup> ]	$\sigma_1$ [MPa]	$\sigma_2$ [MPa]	m	$m_{ave}(\epsilon, T)$
500	0.05	0.0001	0.0005	7.75	8.85	0.082	0.082
500	0.05	0.0001	0.001	7.75	9.23	0.075	
500	0.05	0.0001	0.005	7.75	10.65	0.081	

500	0.05	0.0005	0.005	8.85	10.65	0.080	
500	0.05	0.001	0.005	9.23	10.65	0.089	
500	0.1	0.0001	0.0005	7.70	9.07	0.102	0.091
500	0.1	0.0001	0.001	7.70	9.38	0.086	
500	0.1	0.0001	0.005	7.70	10.94	0.090	
500	0.1	0.0005	0.005	9.07	10.94	0.082	
500	0.1	0.001	0.005	9.38	10.94	0.096	
500	0.2	0.0001	0.0005	7.54	9.12	0.118	0.102
500	0.2	0.0001	0.001	7.54	9.45	0.099	
500	0.2	0.0001	0.005	7.54	11.19	0.101	
500	0.2	0.0005	0.005	9.12	11.19	0.089	
500	0.2	0.001	0.005	9.46	11.19	0.105	
500	0.3	0.0001	0.0005	7.31	8.96	0.126	0.110
500	0.3	0.0001	0.001	7.31	9.13	0.096	
500	0.3	0.0001	0.005	7.31	11.14	0.108	
500	0.3	0.0005	0.005	8.96	11.14	0.094	
500	0.3	0.001	0.005	9.13	11.14	0.123	

These average m-values give the strain rate sensitivity of Al1050-H14 alloy at 200 °C, 300 °C, and 500 °C to be approximately 0.07, 0.12 and 0.1, respectively. The most practical methods to calculate m-value are:

- Obtaining m-value from  $\ln(\sigma_t) - \ln(\dot{\epsilon}_t)$  curve,
- Calculating m-value using change in the strain rate,
- Using the SR tests to determine m-value.

Considering the experimental data in Fig. 1, the first measuring method is employed in this paper to calculate the strain rate of commercial AA1050-H14 (See more detail in Allazadeh (2018: 9009)). In this method, m-value is the slope of the  $\ln(\sigma_t) - \ln(\dot{\epsilon}_t)$  plot, which may be measured either graphically or via differentiation of a curve fitting procedure for the true stress-strain rate plot. Consequently, one can calculate the m-value in the  $\ln(\sigma_t) - \ln(\dot{\epsilon}_t)$  plot according to the standard method defined in equation (1) with the following equation,

$$m|_{T=T_0, \epsilon=\epsilon_0} = \frac{\ln(\sigma_1/\sigma_2)}{\ln(\dot{\epsilon}_1/\dot{\epsilon}_2)} \quad (6)$$

Where the values of stress  $\sigma_1$  and  $\sigma_2$  at the temperature  $T_0$  and the strain  $\epsilon_0$  correspond to  $\dot{\epsilon}_1$  and  $\dot{\epsilon}_2$ , respectively. Then, m-value is the slope of the line connecting the stress values related to the uniaxial tensile tests carried under loading with different predefined constant strain rates.

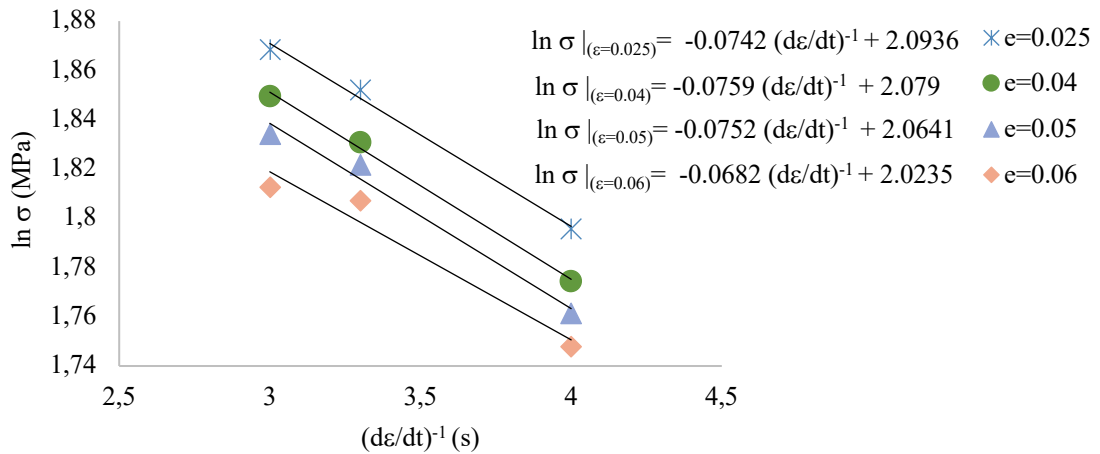


Fig 2. Variation of flow stress with respect to strain rate at 200 °C about different strains within the creep zone before necking onset

It is more convenient to plot  $\ln(\sigma_t) - \ln(1/\dot{\epsilon}_t)$  curves instead of  $\ln(\sigma_t) - \ln(\dot{\epsilon}_t)$  curves to present the effect of strain rates on the stress flow in the quadrant-I of the coordinate system. Hence, the  $m$ -value is negative value for the slope of  $\ln(\sigma_t) - \ln(1/\dot{\epsilon}_t)$  curve. Fig. 2, Fig. 3, and Fig. 4 present  $\ln(\sigma_t) - \ln(1/\dot{\epsilon}_t)$  plots for the selected strains in Table 2, Table 3, and Table 4, respectively. In these figures, the  $m$ -value can be approximated by the negative of the slope of linear trend line related to the dependent parameter  $\ln(\sigma_t)$ , and independent parameter  $\ln(1/\dot{\epsilon}_t)$ . The corresponding equations of the linear trend line shows the sensitivity of the stress flow in response to changes in the strain rate for each strain with the accuracy of near to the unity. It is also possible to obtain the  $m$ -value of AA1050-H14 from the flow stress data extracted from Fig. 1 at 100 °C forming temperature. The computed  $m$ -value at 100 °C is 0.04 for warm uniaxial tensile testing temperature at strain rate  $0.001 \text{ s}^{-1}$  and  $0.005 \text{ s}^{-1}$  about strain of 5%. Moreover, Figs. 2 and 3 reveal that  $m$ -value is almost constant within the plastic deformation region for formation temperature up to 300 °C while  $m$ -value increases by %20 as the probe strain in the plastic deformation region gets close to necking onset for formation at 500 °C. Fig. 5 depicts the changes in AA1050-H14  $m$ -value as a function of temperature in vicinity of 5% strain in the stress flow curve of the material. A maximum tip can be seen in the graph of Fig. 5 which might be related to the rate of the formation and accumulation of the dislocations as function of the external load to the stress relief due to the recrystallization and recovery in function of time.

One can insert the data in Table 2, Table 3, and Table 4 into Equations (4) and (5) to simulate the formation of Al1050 sheet using time-hardening and strain-hardening power law, respectively, in commercial finite element software packages such as ABAQUS.

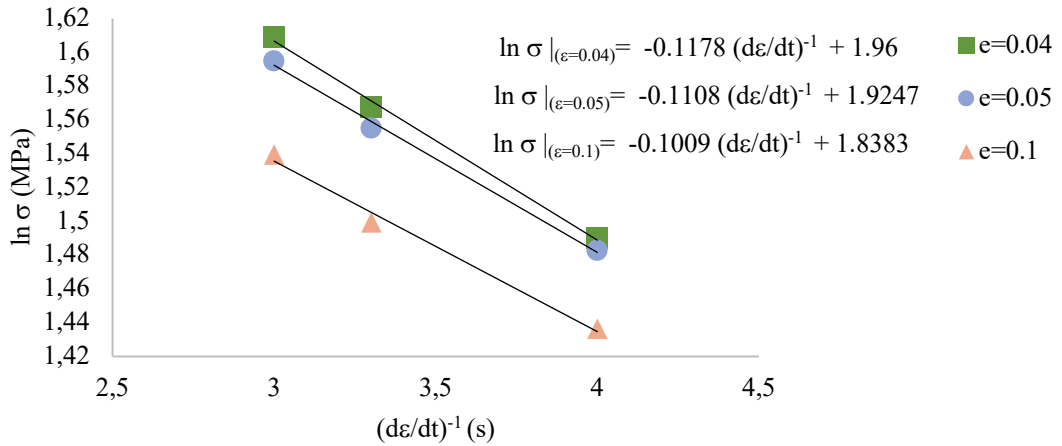


Fig 3. Variation of flow stress with respect to strain rate at 300 °C about different strains within the pure plastic zone before necking onset

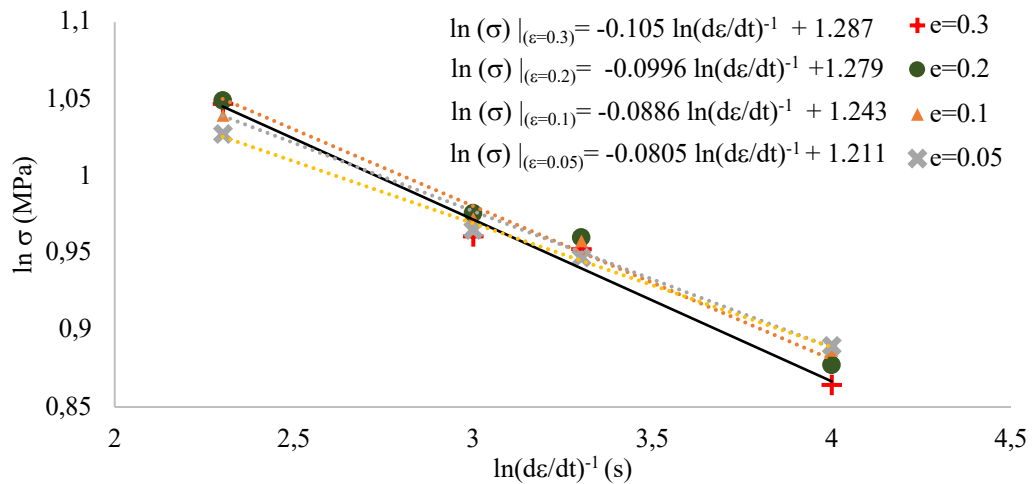


Fig 4. Variation of flow stress with respect to strain rate at 500 °C about different strains within the pure plastic zone before necking onset

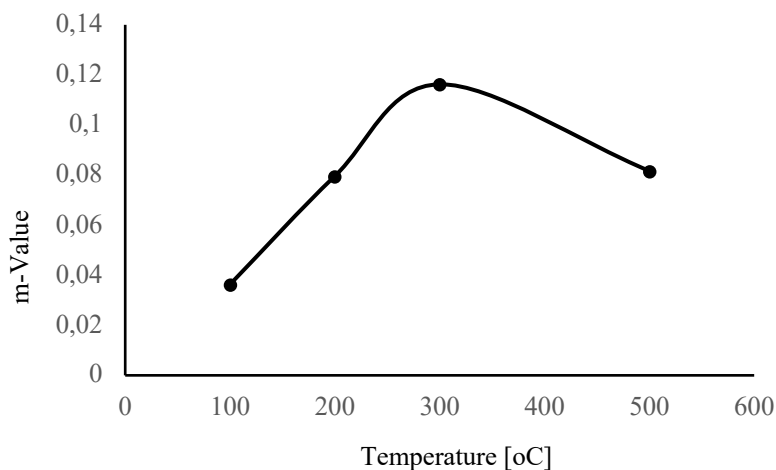


Fig 5. Changes in m-value at strain  $\epsilon=0.05$  in function of temperature

Variation in strain rate and temperature are influencing the flow stress and strain hardening rate (Mishra and Mahoney: 2004). The strain hardening mechanism in

aluminum alloys with face-centered cubic (F.C.C.) structure metal alloys is determined by interaction between the individual dislocations in the plastic flow and the barriers of obstacles, such as precipitation particles or dislocation forest (Abedrabbo et al., 2007: 841-875; Nemat-Nasser and Li, 1998: 565). This implies that increasing the strain rate changes the curvature of the strain hardening for FCC metals (Liang and Khan, 1999: 963-980). However, aluminum dislocation drag coefficient is affected by both temperature and strain of dynamic loading (Kumar et al., 1968: 1189; Campbell and Ferguson, 1970: 63-82). This fact exhibits itself by dependency of the thermally activated stress on strain rate such that the dislocations movement can pass more barriers in the microstructure as the temperature increases. This phenomena is known as thermal softening effect. Researchers have found the thermal softening effect in many polycrystalline materials (Khan, 2007a: 931-950; Khan, 2007b: 1105-1125; Khan and Meredith, 2010: 189-203; Sung et al., 2010: 1746). Consequently, the optimum strain rate sensitivity is a balance between the strain hardening and thermal softening.

Moreover, research results showed that as the strain rates decreases, the  $m$ -value increases (Ivanov and Naydenkin, 2014: 313). Suo et al. (2013: 1-10) studied the temperature influence on  $m$ -value for FCC structure metals and concluded that the forming temperature has inverse relationship with flow stress, and subsequently, direct relationship with  $m$ -value. However, Primorac et al. (2015: 296-302) showed that FCC structure metal may have a maximum  $m$ -value as result of altering intrinsic material properties caused by microstructure modifications. Similar phenomena can be observed in Fig. 5 about 300 °C forming temperature.

Fine-grained microstructure facilitates grain-boundary migration better than coarse-grained materials (Hu et al., 1995: 223-229). Coarse grain structure causes the material to be almost strain rate independent, while finer grain structure makes the material to possess higher  $m$ -value (Hallberg et al., 2010: 1126). Sherby and Wadsworth (1984: 21-78) have stated that the inverse proportional effect of strain rate to the grain size may raise to the second or third power relationship. It was demonstrated that it could be possible to obtain  $m$ -value of 0.04 at the ambient temperature instead of at 100 °C for UFG AA1050 by implementing 2 cycles ARB and SR processes (Mohebbi and Akbarzadeh, 2017: 167-176). It was claimed that the deformation may improve the  $m$ -value by increasing the grain diffusion and grain sliding (Ivanov and Naydenkin, 2014: 313-321). Most metals and alloys have strain rate sensitivity index less than 0.2, whereas typical superplastic alloys  $m$ -values are above 0.33 (Hu et al., 1995: 223-229). It is known that deforming mechanism by dislocation slip causes low strain-rate sensitivity and exhibiting an apparent threshold stress. Furthermore, it is suggested that the grain-boundary sliding mechanism has less contribution in threshold stress than the dislocation creep mechanism in case of low  $m$ -value (Nieh et al., 1997: 145-153). Thereof, AA1050 sheets` applications in the industry can be boosted by enhancing its  $m$ -value using combination of the grain refinements techniques.

Researches have studied the microstructure evolution of AA1050 after application of 50% rolling reduction, using optical microscopy (OM) and scanning electron microscopy (SEM) (Mhedhbi et al., 2017: 2974). These studies showed the elongation of the grains with respect to the rolling direction. The average grain size of AA1050-H14 in the centre of the rolled sheet was reported to be between 26  $\mu\text{m}$  (Qiao and Starink, 2009: 52-58) to 29  $\mu\text{m}$  (Hallberg, 2013: 260-272), and therefore, it has relatively coarse grains and it does not possess superplastic attribute. According to the literature (Krajewski and

Schroth, 2011: 272-303), the forming behaviour of commercial AA1050 is dictated rather by dislocation creep deformation mechanism than grain boundary sliding.

### Conclusion

The strain rate sensitivity was calculated for commercial AA1050H-14 from the uniaxial tensile test experimental results presented in Fig. 1. Creep law governing equation was utilized to determine the strain rate sensitivity of AA1050 by creep model constants derived via the expressions in the appendices. Furthermore, the experimental data in Fig. 1 were plotted in  $\ln(\sigma_t) - \ln(\dot{\epsilon}_t)$  curves and  $m$  value was determined as the slope to the trend line for all experimental data at a specific temperature for a predefined strain. Appendices B and C demonstrated the calculation procedure to map the creep law equation to Bailey-Norton law time hardening as well as strain hardening governing equations, respectively.

The  $m$ -value of AA1050 was calculated using warm uniaxial loading at 100 °C, 200 °C, 300 °C, and 500 °C for different strain rate, about several selected strains within the plastic formation region before the onset of necking phenomena. The average  $m$ -value of AA1050-H14 was found to be approximately 0.04, 0.07, 0.12 and 0.1 at 100 °C, 200 °C, 300 °C, and 500 °C forming temperatures, respectively. Strain rate sensitivity values were compared with the slope of linear trend line in  $\ln(\sigma_t)$  versus  $\ln(1/\dot{\epsilon}_t)$  plots for all tested strain rates at different temperature about the same plastic strains. The results revealed that the dislocation creep may be the dominated forming mechanism of commercial AA1050. Evaluation of the  $m$ -value curve at different temperature showed that optimum AA1050 forming parameter was 300 °C for stress flow curve with strain rate of 0.0005 s<sup>-1</sup> about 4% creep strain. It was also discussed that AA1050 applications in the industry can be promoted by increasing its  $m$ -value index using combination of the grain refinements techniques.

The results can be used to optimise the forming parameters of AA1050 in the industry and to assist the researchers to analyse the creep behaviour of commercial AA1050. The recent trend in light weighting industry is to consolidate parts in components using relatively light and cheap material. AA1050  $m$ -value provides one of the important manufacturing parameter to make cheap and complex shape component by gas forming process.

### Acknowledgement

This research has been financially supported by the High Value Manufacturing (HVM) Catapult undertaken at the Advanced Forming Research Centre (AFRC) of the University of Strathclyde.

### References

- Aalco Metals Ltd. (2011). Aalco Metals Ltd Aluminium Alloy 1050 H14 57. Available at: <https://pdfslide.net/documents/aalco-metals-ltd-aluminium-alloy-1050-h14-57.html>
- Aalco Metals Ltd. (2019). Aluminium Alloy 1050A H14 Sheet. Available at: [www.aalco.co.uk/datasheets/Aalco-Metals-Ltd\\_Aluminium-Alloy-1050A-H14-Sheet\\_57.pdf.ashx](http://www.aalco.co.uk/datasheets/Aalco-Metals-Ltd_Aluminium-Alloy-1050A-H14-Sheet_57.pdf.ashx)
- Abedrabbo, N., Pourboghraat, F., Carsley, J. (2007). Forming of AA5182-O and AA5754-O at elevated temperatures using coupled thermo-mechanical finite element

models. International Journal of Plasticity, 23, 841-875.  
<https://doi.org/10.1016/j.ijplas.2006.10.005>

Afshin, E., Kadkhodayan, M. (2015). An experimental investigation into the warm deep-drawing process on laminated sheets under various grain sizes. Materials and Design, 87, 25-35. <https://doi.org/10.1016/j.matdes.2015.07.061>

Allazadeh, M.R. (2018). Analysing the Effect of Strain Rate and Temperature on the Flow Stress in AA1050 Sheet Using 2448 Standard. Journal of Multidisciplinary Engineering Science and Technology (JMEST), 5(11), 9009-9015. Available at: <https://strathprints.strath.ac.uk/id/eprint/66204>

Bae, D., Ghosh, A.K. (2000). Grain size and temperature dependence of superplastic deformation in an Al–Mg alloy under isostructural condition. Acta materialia, 48(6), 1207-1224. [https://doi.org/10.1016/S1359-6454\(99\)00445-0](https://doi.org/10.1016/S1359-6454(99)00445-0)

Betten, J. (2008). Creep Mechanics. Berlin: Springer.

Bolt, P., Lamboo, N., Rozier, P. (2001). Feasibility of warm drawing of aluminium products. J. Mater. Process. Technol., 115, 118-121. [https://doi.org/10.1016/S0924-0136\(01\)00743-9](https://doi.org/10.1016/S0924-0136(01)00743-9)

Campbell, J.D., Ferguson, W.G. (1970). The temperature and strain-rate dependence of the shear strength of mild steel. Philosophical Magazine, 81, 63-82. <https://doi.org/10.1080/14786437008238397>

Chen, I.Y., Clausen, A.H., Hopperstad, O.S., Langseth, M. (2009). Stress-strain behaviour of aluminium alloys at a wide range of strain rates. International Journal of Solids and Structures, 46(21), 3825-3835. <https://doi.org/10.1016/j.ijsolstr.2009.07.013>

Demirci, H.I., Yaşar, M., Demiray, K., Karali, M. (2008). The theoretical and experimental investigation of blank holder forces plate effect in deep drawing process of AL 1050 material. Mater. Des., 29, 526-532. <https://doi.org/10.1016/j.matdes.2007.01.008>

Grupo Andaluca. (2013). Aluminium alloy 1050. Available at: [http://grupoandalucia.org/pdf/aluminium\\_1050.pdf](http://grupoandalucia.org/pdf/aluminium_1050.pdf)

Hallberg, H. (2010). Mathias Wallin, Matti Ristinmaa, Modeling of continuous dynamic recrystallization in commercial-purity aluminium. Materials Science and Engineering A, 572, 1126-1134. <https://doi.org/10.1016/j.msea.2009.09.043>

Hallberg, H. (2013). Influence of process parameters on grain refinement in AA1050 aluminum during cold rolling. International Journal of Mechanical Sciences, 66, 260-272. <https://doi.org/10.1016/j.ijmecsci.2012.11.016>

Hamilton, C.H., Ghosh, A.K., Wert, J.A. (1985). Superplasticity in engineering alloys: a review. In Metals forum, 8(4), 172-190.

Hu, W., Ponge, D., Gottstein, G. (1995). Origin of Grain Boundary Motion during Diffusion Bounding by Hot Pressing. Mater. Sci. Eng. A, 190(1-2), 223-229. [https://doi.org/10.1016/0921-5093\(94\)09600-2](https://doi.org/10.1016/0921-5093(94)09600-2)

Huang, S., Khan, A.S. (1992). Modeling the mechanical behavior of 1100-0 aluminum at different strain rates by the Bodner-Partom model. International Journal of Plasticity, 8, 501-517. [https://doi.org/10.1016/0749-6419\(92\)90028-B](https://doi.org/10.1016/0749-6419(92)90028-B)

Ivanov, K.V., Naydenkin, E.V. (2014). Tensile behavior and deformation mechanisms of ultrafine-grained aluminum processed using equal-channel angular pressing. Materials Science and Engineering: A, 606, 313-321. <https://doi.org/10.1016/j.msea.2014.03.114>

Khan, A.S., Kazmi, R., Farrokh, B. (2007a). Multiaxial and non-proportional loading responses, anisotropy and modeling of Ti–6Al–4V titanium alloy over wide ranges of strain rates and temperatures. *International Journal of Plasticity*, 23, 931-950. <https://doi.org/10.1016/j.ijplas.2006.08.006>

Khan, A.S., Kazmi, R., Farrokh, B., Zupan, M. (2007b). Effect of oxygen content and microstructure on the thermo-mechanical response of three Ti–6Al–4V alloys: experiments and modeling over a wide range of strain-rates and temperatures. *International Journal of Plasticity*, 23, 1105-1125. <https://doi.org/10.1016/j.ijplas.2006.10.007>

Khan, A.S., Liu, H. (2012). Variable strain rate sensitivity in an aluminum alloy: Response and constitutive modelling. *International Journal of Plasticity*, 36, 1-14. <https://doi.org/10.1016/j.ijplas.2012.02.001>

Khan, A.S., Meredith, C.S. (2010). Thermo-mechanical response of Al 6061 with and without equal channel angular pressing (ECAP). *International Journal of Plasticity*, 26, 189-203. <https://doi.org/10.1016/j.ijplas.2009.07.002>

Kima, K., Kanga, W., Leeb, S.-I., Parkc, S.H., Yoond, J. (2017). Microstructural evolution and enhancement of mechanical properties of Al1050 by tubular channel angular extrusion. *Materials Science & Engineering A*, 696, 26-32. Available at: <https://www.infona.pl/resource/bwmeta1.element.elsevier-d0f9971d-5587-3cd6-94a4-5f6449687fa1/tab/disciplines>

Krajewski, P.E., Schroth, J.G. (2011). *Quick Plastic Forming of Aluminium Alloys, Superplastic Forming of Advanced Metallic Materials - Methods and Applications*. Cambridge: Woodhead Publishing.

Kumar, A., Hauser, F.E., Dorn, J.E. (1968). Viscous drag on dislocations in aluminum at high strain rates. *Acta Metallurgica*, 9 (16), 1189-1197. [https://doi.org/10.1016/0001-6160\(68\)90054-0](https://doi.org/10.1016/0001-6160(68)90054-0)

Lademo, O., Engler, O., Aegerter, J., Berstad, T., Benallal, A., Hopperstad, O.S. (2010). Strain-Rate Sensitivity of Aluminum Alloys AA1200 and AA3103. *ASME. J. Eng. Mater. Technol.*, 132(4), 041007. <https://doi.org/10.1115/1.4002160>

Liang, R., Khan, A.S. (1999). A critical review of experimental results and constitutive models of BCC and FCC metals over a wide range of strain rates and temperatures. *International Journal of Plasticity*, 15, 963-980. [https://doi.org/10.1016/S0749-6419\(99\)00021-2](https://doi.org/10.1016/S0749-6419(99)00021-2)

Majidi, O., Jahazi, M., Bombardier, N., Samue, E. (2017). Variation of strain rate sensitivity index of a superplastic aluminum alloy in different testing methods. *AIP Conference Proceedings*, 1896, 020022. <https://doi.org/10.1063/1.5007979>

May, D.L., Gordon, A.P., Segletes, D.S. (2013). The application of the NORTON-BAILEY law for creep prediction through power law regression. *Proceedings of ASME Turbo Expo 2013: Turbine Technical Conference and Exposition, GT2013-96008*, San Antonio, Texas, USA. <https://doi.org/10.1115/GT2013-96008>

Metals4U LTD. (2019). 1050A Aluminium. Available at: [www.metals4u.co.uk](http://www.metals4u.co.uk)

Mhedhbi, M., Khlif, M., Bradai, C. (2017). Investigations of microstructural and mechanical properties evolution of AA1050 alloy sheets deformed by cold-rolling process and heat treatment annealing. *JMES*, 8(8), 2967-2974. Available at: [https://www.researchgate.net/publication/318513127\\_Investigations\\_of\\_microstructural\\_and\\_mechanical\\_properties\\_evolution\\_of\\_AA1050\\_alloy\\_sheets\\_deformed\\_by\\_cold-rolling\\_process\\_and\\_heat\\_treatment\\_annealing](https://www.researchgate.net/publication/318513127_Investigations_of_microstructural_and_mechanical_properties_evolution_of_AA1050_alloy_sheets_deformed_by_cold-rolling_process_and_heat_treatment_annealing)

Mishra, R.S., Mahoney, M.W. (2004). Metal Superplasticity Enhancement and Forming Process. U.S. Patents, US 6,712,916 B2. Available at: [https://scholarsmine.mst.edu/cgi/viewcontent.cgi?article=2576&context=matsci\\_eng\\_fac\\_work](https://scholarsmine.mst.edu/cgi/viewcontent.cgi?article=2576&context=matsci_eng_fac_work)

Mohebbi, M.S., Akbarzadeh, A. (2017). Development of equations for strain rate sensitivity of UFG aluminum as a function of strain rate. *International Journal of Plasticity*, 90, 167-176. <https://doi.org/10.1016/j.ijplas.2017.01.003>

Morais, J.M.S. (2014). Mechanical Behavior of AA1050 at High Strain Rates, Master Degree in Mechanical Engineering, Instituto Superior Técnico, Universidade Técnica de Lisboa. Available at: [https://fenix.tecnico.ulisboa.pt/downloadFile/1970719973965863/Dissertacao\\_67795.pdf](https://fenix.tecnico.ulisboa.pt/downloadFile/1970719973965863/Dissertacao_67795.pdf)

Mukherjee, A.X. (1993). *Materials Science and Technology*. Weinheim: VCH Publishers.

Nazzal, M.A., Khraisheh, M.K., Abu-Farha, F.K. (2007). The effect of strain rate sensitivity evolution on deformation stability during superplastic forming. *Journal of Materials Processing Technology*, 191, 189-192. <https://doi.org/10.1016/j.jmatprotec.2007.03.097>

Nemat-Nasser, S., Li, Y. (1998). Flow stress of F.C.C. polycrystals with application to OFHC Cu *Acta Materialia*, 46 (2), 565-577. [https://doi.org/10.1016/S1359-6454\(97\)00230-9](https://doi.org/10.1016/S1359-6454(97)00230-9)

Nieh, T., Wadsworth, J., Sherby, O. (1997). Fine structure superplastic composites and laminates. In *Superplasticity in Metals and Ceramics* (Cambridge Solid State Science Series, pp. 145-153). Cambridge: Cambridge University Press. <https://doi.org/10.1017/CBO9780511525230.009>

Picua, R.C., Vinczeb, G., Ozturka, F., Graciob, J.J., Barlatb, F., Maniatty, A.M. (2005). Strain rate sensitivity of the commercial aluminum alloy AA5182-O. *Materials Science and Engineering A*, 390, 334-343.

Primorac, M.-M., Abad, M.D., Hosemann, P., Kreuzeder, M., Maier, V., Kiener, D. (2015). Elevated temperature mechanical properties of novel ultra-fine grained Cu–Nb composites. *Materials Science & Engineering A*, 625, 296-302. <https://doi.org/10.1016/j.msea.2014.12.020>

Qiao, X.G., Starink, M.J. (2009). N. Gao, Hardness inhomogeneity and local strengthening mechanisms of an Al1050 aluminium alloy after 1 pass of equal channel angular pressing. *Materials Science and Engineering A*, 52-58. <https://doi.org/10.1016/j.msea.2009.01.051>

San-Vicente, J.L. (2004). Creep Simulations with ABAQUS: Super Plastic Forming. FE Issues Related to Creep and Viscoelasticity. A summary report of the FENet Durability and Life Extension (DLE) workshop in Majorca, Spain, 25th - 26th March 2004. Available at:

[https://old.nafems.org/downloads/FENet\\_Meetings/Majorca\\_Spain\\_Mar\\_2004/FENET\\_Majorca\\_March2004\\_DLE\\_SanVicente.pdf](https://old.nafems.org/downloads/FENet_Meetings/Majorca_Spain_Mar_2004/FENET_Majorca_March2004_DLE_SanVicente.pdf)

Sherby, O.D., Wadsworth, J. (1984). Development and Characterization of Fine Grain Superplastic Material. In: G. Krauss (Ed.), *Deformation, Processing and Structure* (pp. 355-389). Ohio: ASM, Metal Park.

Smiths Metal Centres. (2018). 1050A (S1B) Technical Datasheet. Available at: <https://www.smithmetal.com/pdf/aluminium/1xxx/1050a.pdf>

Sung, J.H., Kim, J.H., Wagoner, R.H. (2010). A plastic constitutive equation incorporating strain, strain-rate, and temperature. *International Journal of Plasticity*, 26, 1746-1771. <https://doi.org/10.1016/j.ijplas.2010.02.005>

Suo, T., Li, Yu., Zhao, F., Fan, X., Guo, W. (2013). Compressive behavior and rate-controlling mechanisms of ultrafine grained copper over wide temperature and strain rate ranges. *Mechanics of Materials*, 61, 1-10. <https://doi.org/10.1016/j.mechmat.2013.02.003>

Totten, G.E., Mackenzie, D.S. (2003). *Handbook of aluminium, Superplastic forming*. NewYork-Bassel: Macel Dekker, Inc.

Zheng, K., Politis, D.J., Wang, L., Lin, J. (2018). A review on forming techniques for manufacturing lightweight complex-shaped aluminium panel components. *International Journal of Lightweight Materials and Manufacture*, 1(2), 55-80.

## Appendices

### Appendix A

Time hardening equation for creep strain ( $\varepsilon^{cr}$ ) is expressed as following:

$$\varepsilon^{cr} = A\sigma^n t^k \quad (7)$$

The time factor of the above equation can be defined as:

$$t = \left(\frac{\varepsilon^{cr}}{A\sigma^n}\right)^{\frac{1}{k}} \quad (8)$$

Differentiating (7) with respect to time t gives the strain rate of time hardening equation, i.e. (4):

$$\dot{\varepsilon}^{cr} = kA\sigma^n t^{(k-1)} \quad (9)$$

Plugging the time factor into equation (9) gives:

$$\dot{\varepsilon}^{cr} = kA\sigma^n \left[\left(\frac{\varepsilon^{cr}}{A\sigma^n}\right)^{\frac{1}{k}}\right]^{(k-1)} = kA^{1-\frac{k-1}{k}}\sigma^n(1-\frac{k-1}{k}) (\varepsilon^{cr})^{\frac{k-1}{k}} = kA^{\frac{1}{k}}\sigma^{\frac{n}{k}} (\varepsilon^{cr})^{\frac{k-1}{k}} \quad (10)$$

Make the two sides of equation to the power of m/n and rearranging the equation to have expression for stress gives:

$$\sigma = \left(\frac{1}{k}\right)^{\frac{k}{n}} A^{-\frac{1}{n}} (\dot{\varepsilon}^{cr})^{\frac{k}{n}} (\varepsilon^{cr})^{-\frac{k-1}{k}\frac{k}{n}} = \left(\frac{1}{k}\right)^{\frac{k}{n}} A^{-\frac{1}{n}} (\dot{\varepsilon}^{cr})^{\frac{k}{n}} (\varepsilon^{cr})^{\frac{1-k}{n}} \quad (11)$$

It is easy to obtain  $\varepsilon^{cr} = \frac{1}{k} t \dot{\varepsilon}^{cr}$  by comparing (7) and (9). Then, (11) can be modified to the following expression:

$$\sigma = \frac{1}{k} A^{-\frac{1}{k}} (\dot{\varepsilon}^{cr})^{\frac{k}{n}} \left(\frac{1}{k} t \dot{\varepsilon}^{cr}\right)^{\frac{1-k}{n}} = \left(\frac{1}{k}\right)^{\frac{k+1-k}{n}} A^{-\frac{1}{n}} t^{\frac{1-k}{n}} (\dot{\varepsilon}^{cr})^{\frac{k}{n}} (\dot{\varepsilon}^{cr})^{\frac{1-k}{n}} \quad (12)$$

So the stress expression becomes:

$$\sigma = (k)^{-\frac{1}{n}} A^{-\frac{1}{n}} t^{\frac{1-k}{n}} (\dot{\epsilon}^{cr})^{\frac{1}{n}} = B t^{\frac{1-k}{n}} (\dot{\epsilon}^{cr})^{\frac{1}{n}} \quad (13)$$

Where coefficient B is  $B = (kA)^{\frac{1}{n}}$ . Taking natural logarithm from both sides of the equation gives:

$$\ln \sigma = \ln \left( B t^{\frac{1-k}{n}} (\dot{\epsilon}^{cr})^{\frac{1}{n}} \right) = \ln \left( B t^{\frac{1-k}{n}} \right) + \ln (\dot{\epsilon}^{cr})^{\frac{1}{n}} \quad (14)$$

Taking partial differential from both sides with respect to  $\ln(\dot{\epsilon}^{cr})$ , gives:

$$\frac{\partial \ln \sigma}{\partial \ln (\dot{\epsilon}^{cr})} = \frac{1}{n} \quad (15)$$

Comparing the last equation with the standard definition of m-value, i.e. equation (2), shows that stress exponent, n, has value equivalent to inverse of m-value, i.e.  $n=1/m$ .

#### Appendix B

The alternative form of the Norton-Bailey law can be extracted from (4) by replacing constants  $A'$ ,  $m'$ ,  $n'$  in (9):

$$\dot{\epsilon}^{cr} = k A^{\frac{1}{k}} \sigma^{\frac{n}{k}} t^{(k-1)} = A' \sigma^{n'} t^{k'} \quad (16)$$

Where  $A' = k A^{\frac{1}{k}}$ ,  $n' = \frac{n}{k}$  and  $k'=k-1$ . Then, the stress can be expressed as:

$$\sigma = A'^{-\frac{1}{n'}} t^{\frac{n'}{k'}} \dot{\epsilon}^{cr \frac{1}{n'}} \quad (17)$$

Taking natural logarithm of (17) gives:

$$\ln \sigma = \ln A'^{-\frac{1}{n'}} + \ln t^{\frac{n'}{k'}} + \ln \dot{\epsilon}_{cr}^{\frac{1}{n'}} = \ln \left( A'^{-\frac{1}{n'}} \right) + \ln \left( t^{\frac{n'}{k'}} \right) + \frac{1}{n'} \ln (\dot{\epsilon}^{cr}) \quad (18)$$

Differentiate both sides of (18) with respect to  $\ln (\dot{\epsilon}^{cr})$ , gives the m-value as:

$$m = \frac{\partial \ln \sigma}{\partial \ln (\dot{\epsilon}^{cr})} = \frac{1}{n'} \quad (19)$$

Considering two points in the stress flow curve at a specified strain rate of  $\dot{\epsilon}_*$

$$\text{Point \#1: } \dot{\epsilon}_* = A' \sigma_1^{n'} t_1^{k'} \quad (20)$$

$$\text{Point \#2: } \dot{\epsilon}_* = A' \sigma_2^{n'} t_2^{k'} \quad (21)$$

Comparing (20) and (21) gives,

$$\left. \begin{aligned} \dot{\epsilon}_* &= A' \sigma_1^{n'} t_1^{k'} \\ \dot{\epsilon}_* &= A' \sigma_2^{n'} t_2^{k'} \end{aligned} \right\} \rightarrow \sigma_1^{n'} t_1^{k'} = \sigma_2^{n'} t_2^{k'} \rightarrow \left( \frac{\sigma_1}{\sigma_2} \right)^{n'} = \left( \frac{t_2}{t_1} \right)^{k'} \quad (22)$$

Taking logarithm from both sides of equation (22):

$$\ln\left(\frac{\sigma_1}{\sigma_2}\right)^{n'} = \ln\left(\frac{t_2}{t_1}\right)^{k'} \rightarrow n' \ln \frac{\sigma_1}{\sigma_2} = k' \ln \frac{t_2}{t_1} \quad (23)$$

Plugging value of  $n'$  in terms of  $m$ -value in equation (23) gives the value of constant  $k'$  as:

$$\frac{1}{m} \ln \frac{\sigma_1}{\sigma_2} = k' \ln \frac{t_2}{t_1} \rightarrow k' = \frac{1}{m} \frac{\ln \sigma_1 / \sigma_2}{\ln t_2 / t_1} \quad (24)$$

The value of  $A'$  may defined from equation (20) or (21) as:

$$A' = \sigma_1^{-n'} t^{-k'} \dot{\varepsilon}_* = \dot{\varepsilon}_* \sigma_1^{-\frac{1}{m} t^{-\frac{1}{m} \frac{\ln \sigma_1 / \sigma_2}{\ln t_2 / t_1}}} = \dot{\varepsilon}_* \left[ \sigma_1 t^{\frac{\ln \sigma_1 / \sigma_2}{\ln t_2 / t_1}} \right]^{-\frac{1}{m}} \quad (25)$$

### Appendix C

The strain hardening equation is derived from time hardening equation via following computational method. Calculating time parameter from time hardening equation ,i.e. (16), gives:

$$\dot{\varepsilon}^{cr} = A' \sigma^{n'} t^{k'} \rightarrow t = \left( \frac{\dot{\varepsilon}^{cr}}{A' \sigma^{n'}} \right)^{\frac{1}{k'}} \quad (26)$$

Equation (16) can be rewritten as:

$$\frac{d\varepsilon}{dt} = A' \sigma^{n'} t^{k'} \rightarrow d\varepsilon = (A' \sigma^{n'} t^{k'}) dt \quad (27)$$

Taking integral from both sides gives:

$$\int d\varepsilon = \int (A' \sigma^{n'} t^{k'}) dt \rightarrow \varepsilon = A' \sigma^{n'} \frac{t^{k'+1}}{k'+1} \quad (28)$$

Inserting (26) into (28) gives

$$\varepsilon = A' \sigma^{n'} \frac{1}{k'+1} \left[ \left( \frac{\dot{\varepsilon}}{A' \sigma^{n'}} \right)^{\frac{1}{k'}} \right]^{k'+1} \rightarrow (k' + 1)\varepsilon = A'^{\left(1 - \frac{k'+1}{k'}\right)} (\sigma^{n'})^{\left(1 - \frac{k'+1}{k'}\right)} \dot{\varepsilon}^{\left(\frac{k'+1}{k'}\right)} = (A' \sigma^{n'})^{\left(\frac{1}{k'}\right)} \dot{\varepsilon}^{\left(\frac{k'+1}{k'}\right)} \quad (29)$$

So,

$$(k' + 1)\varepsilon = \left[ (A' \sigma^{n'})^{-1} \dot{\varepsilon}^{k'+1} \right]^{\frac{1}{k'}} \rightarrow [(k' + 1)\varepsilon]^{k'} = (A' \sigma^{n'})^{-1} \dot{\varepsilon}^{k'+1} \quad (30)$$

Hence,

$$A \sigma^{n'} [(k' + 1)\epsilon]^{k'} = \dot{\epsilon}^{k'+1} \quad (31)$$

So, the strain rate hardening equation is:

$$\dot{\epsilon} = [A \sigma^{n'} [(k' + 1)\epsilon]^{k'}]^{\frac{1}{k'+1}} \quad (32)$$

The values of  $A$ ,  $n'$ , and  $k'$  are calculated by following method. The stress can be expressed using equation (31) as:

$$\sigma^{n'} = \frac{\dot{\epsilon}^{k'+1}}{A [(k'+1)\epsilon]^{k'}} \rightarrow \sigma = \left(\frac{1}{A}\right)^{\frac{1}{n'}} [(k' + 1)\epsilon]^{\left(\frac{k'}{n'}\right)} \dot{\epsilon}^{\left(\frac{k'+1}{n'}\right)} \quad (33)$$

Taking logarithm from both sides of (33):

$$\ln \sigma = \frac{1}{n'} \ln \frac{1}{A} - \frac{k'}{n'} \ln((k' + 1)\epsilon) + \left(\frac{k'+1}{n'}\right) \ln \dot{\epsilon} = \frac{1}{n'} \ln \frac{1}{A} - \frac{k'}{n'} [\ln(k' + 1) + \ln(\epsilon)] + \left(\frac{k'+1}{n'}\right) \ln \dot{\epsilon} \quad (34)$$

$\dot{\epsilon}$  in the last equation is related to the time derivative of the plastic strain  $\epsilon$  in the flow stress curve, loading with constant strain rate. The strain  $\epsilon$  for m-values calculation is selected after relaxing yield stress and before necking onset, where the true stress- true strain has almost linear relationship (see uniaxial tensile test graphs in Grupo Andaluca (2013) ). Therefore, it is possible to show  $\epsilon = t\dot{\epsilon}$  for the total time of the creep deformation  $t$  of uniaxial tensile test carried at the constant strain rate corresponding to the linear section of the pure plastic flow. Hence, equation (34) can be rewritten as:

$$\begin{aligned} \ln \sigma &= \frac{1}{n'} \ln \frac{1}{A} - \frac{k'}{n'} [\ln(k'+1) + \ln(t\dot{\epsilon})] + \left(\frac{k'+1}{n'}\right) \ln \dot{\epsilon} \\ &= \frac{1}{n'} \ln \frac{1}{A} - \frac{k'}{n'} [\ln(k'+1) + \ln(t) + \ln(\dot{\epsilon})] + \left(\frac{k'+1}{n'}\right) \ln \dot{\epsilon} \end{aligned}$$

$$\ln \sigma = \frac{1}{n'} \ln \frac{1}{A} - \frac{k'}{n'} [\ln(k'+1) + \ln(t) + \ln(\dot{\epsilon})] + \left(\frac{k'+1}{n'}\right) \ln \dot{\epsilon} \quad (35)$$

Taking the partial differentiation with respect to  $\ln(\dot{\epsilon})$  gives:

$$m = \frac{\partial \ln \sigma}{\partial \ln \dot{\epsilon}_{cr}} = \frac{1}{n'} \rightarrow n' = \frac{1}{m} \quad (36)$$

Considering two points in the stress flow curve at a specified strain rate of  $\dot{\epsilon}_*$

Point #1:

$$\dot{\varepsilon}_* = [A \sigma_1^n [(k + 1)\varepsilon_1]^k]^{\left(\frac{1}{k+1}\right)} \quad (37)$$

Point #2:

$$\dot{\varepsilon}_* = [A \sigma_2^n [(k + 1)\varepsilon_2]^k]^{\left(\frac{1}{k+1}\right)} \quad (38)$$

By comparing (37) with (38), the following equation can be deduced:

$$[A \sigma_1^n [(k + 1)\varepsilon_1]^k]^{\left(\frac{1}{k+1}\right)} = [A \sigma_2^n [(k + 1)\varepsilon_2]^k]^{\left(\frac{1}{k+1}\right)} \rightarrow \sigma_1^n [(k + 1)\varepsilon_1]^k = \sigma_2^n [(k + 1)\varepsilon_2]^k \quad (39)$$

Hence,

$$\left(\frac{\sigma_1}{\sigma_2}\right)^n = \left(\frac{\varepsilon_2}{\varepsilon_1}\right)^k \quad (40)$$

Taking natural logarithm from both sides of (39) gives:

$$n \ln \left(\frac{\sigma_1}{\sigma_2}\right) = k \ln \left(\frac{\varepsilon_2}{\varepsilon_1}\right) \quad (41)$$

$k$  is calculated from equation (40) as:

$$k = \frac{n \ln \left(\frac{\sigma_1}{\sigma_2}\right)}{\ln \left(\frac{\varepsilon_2}{\varepsilon_1}\right)} \quad (42)$$

Constant  $A$  can be express using equation (31) as:

$$A = \frac{\dot{\varepsilon}^{k+1}}{\sigma^n [(k+1)\varepsilon]^k} = \dot{\varepsilon}^{k+1} \sigma^{-n} [(k + 1)\varepsilon]^{-k} \quad (43)$$

The value of  $A$  may be obtained by plugging (36) and (42) into (43) as:

$$A = \dot{\varepsilon}_*^{\frac{n \ln \left(\frac{\sigma_1}{\sigma_2}\right)}{\ln \left(\frac{\varepsilon_2}{\varepsilon_1}\right) + 1}} \sigma^{-\frac{1}{m} \left[ \left( \frac{n \ln \left(\frac{\sigma_1}{\sigma_2}\right)}{\ln \left(\frac{\varepsilon_2}{\varepsilon_1}\right)} + 1 \right) \varepsilon_1 \right]^{-\frac{n \ln \left(\frac{\sigma_1}{\sigma_2}\right)}{\ln \left(\frac{\varepsilon_2}{\varepsilon_1}\right)}} \quad (44)$$

$A$ ,  $n$ , and  $k$  give the values of  $A$ ,  $n$ , and  $k$  constants in equations (3) and (7).